ACCOUNTS of chemical research

pubs.acs.org/accounts

Article

Linear Free Energy Relationships for Enzymatic Reactions: Fresh Insight from a Venerable Probe

John P. Richard,* Judith R. Cristobal, and Tina L. Amyes

Cite This: *Acc. Chem. Res.* 2021, 54, 2532–2542

Read Online

ACCESS | Metrics & More | Article Recommendations

CONSPECTUS: Linear free energy relationships (LFERs) for substituent effects on reactions that proceed through similar transition states provide insight into transition state structures. A classical approach to the analysis of LFERs showed that differences in the slopes of Brønsted correlations for addition of substituted alkyl alcohols to ring-substituted 1-phenylethyl carbocations and to the β-galactopyranosyl carbocation intermediate of reactions catalyzed by β-galactosidase provide evidence that the enzyme catalyst modifies the curvature of the energy surface at the saddle point for the transition state for nucleophile addition. We have worked to generalize the use of LFERs in the determination of enzyme mechanisms. The defining property of enzyme catalysts is their specificity for binding the transition state with a much higher affinity than the substrate. Triosephosphate isomerase (TIM), orotidine 5′-monophosphate decarboxylase (OMPDC), and glycerol 3-phosphate dehydrogenase (GPDH) show effective catalysis of reactions of phosphorylated substrates and strong phosphite dianion activation of reactions of phosphodianion truncated substrates, with rate constants k_{cat}/K_m (M^{-1} s^{-1}) and k_{cat}/K_dK_{HPi} (M^{-2} s^{-1}), respectively. Good linear logarithmic correlations, with a slope of 1.1, between these kinetic parameters determined for reactions catalyzed by five or more variant forms of each catalyst are observed, where the protein substitutions are mainly at side chains which function to stabilize the cage complex between the enzyme and substrate. This shows that the enzyme-catalyzed reactions of a whole substrate and substrate pieces proceed through transition states of similar structures. It provides support for the proposal that the dianion binding energy of whole phosphodianion substrates and of phosphite dianion is used to drive the conversion of these protein catalysts from flexible and entropically rich ground states to stiff and catalytically active Michaelis complexes that show the same activity toward catalysis of the reactions of whole and phosphodianion truncated substrates. There is a good linear correlation, with a slope of 0.73, between values of the dissociation constants log K_i for release of the transition state analog phosphoglycolate (PGA) trianion and log k_{cat}/K_m for isomerization of GAP for wild-type and variants of TIM. This correlation shows that the substituted amino acid side chains act to stabilize the complex between TIM and the PGA trianion and that *ca.* 70% of this stabilization is observed at the transition state for substrate deprotonation. The correlation provides evidence that these side chains function to enhance the basicity of the E165 side chain of TIM, which deprotonates the bound carbon acid substrate. There is a good linear correlation, with a slope of 0.74, between the values of $\Delta G^{\ddagger}$ and ΔG° determined by electron valence bond (EVB) calculations to model deprotonation of dihydroxyacetone phosphate (DHAP) in water and when bound to wild-type and variant forms of TIM to form the enediolate reaction intermediate. This correlation provides evidence that the stabilizing interactions of the transition state for TIM-catalyzed deprotonation of DHAP are optimized by placement of amino acid side chains in positions that provide for the maximum stabilization of the charged reaction intermediate, relative to the neutral substrate.

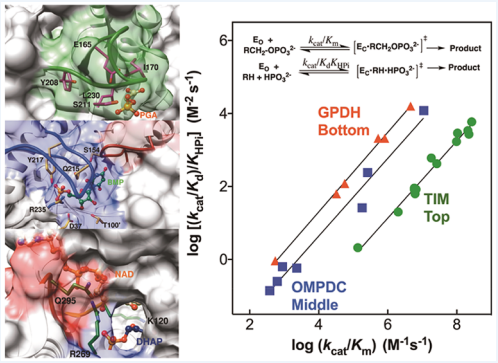

KEY REFERENCES

• Zhai, X.; Amyes, T. L.; Richard, J. P. Role of Loop-Clamping Side Chains in Catalysis by Triosephosphate Isomerase. *J. Am. Chem. Soc.* **2015**, *137*, 15185−15197.[1] *The report of a linear logarithmic correlation between kinetic parameters for wild-type and variant TIM-catalyzed reactions of a whole substrate and substrate pieces. This provides evidence that the two reaction transition states are stabilized by similar interactions with the enzyme.*

• Zhai, X.; Reinhardt, C. J.; Malabanan, M. M.; Amyes, T. L.; Richard, J. P. Enzyme Architecture: Amino Acid Side-Chains That Function To Optimize the Basicity of the Active Site Glutamate of Triosephosphate Isomerase. *J. Am. Chem. Soc.* **2018**, *140*, 8277−8286.[2] *The report of a linear correlation*

Received: March 1, 2021
Published: May 3, 2021

https://doi.org/10.1021/acs.accounts.1c00147
Acc. Chem. Res. 2021, 54, 2532−2542

between dissociation constants log K_i for release of the transition state analog phosphoglycolate trianion from wild-type and variants of TIM and log k_{cat}/K_m for the respective enzyme-catalyzed isomerization reactions of GAP.

- Mydy, L. S.; Cristobal, J.; Katigbak, R.; Bauer, P.; Reyes, A. C.; Kamerlin, S. C. L.; Richard, J. P.; Gulick, A. M. Human Glycerol 3-Phosphate Dehydrogenase: X-Ray Crystal Structures that Guide the Interpretation of Mutagenesis Studies. *Biochemistry* **2019**, *58*, 1061−1073.[3] *The report of a linear logarithmic correlation between kinetic parameters for wild-type and variant GPDH-catalyzed reactions of a whole substrate and substrate pieces. This provides evidence that the two reaction transition states are stabilized by similar interactions with the enzyme.*
- Kulkarni, Y. S.; Amyes, T. L.; Richard, J. P.; Kamerlin, S. C. L. Uncovering the Role of Key Active-Site Side Chains in Catalysis: An Extended Brønsted Relationship for Substrate Deprotonation Catalyzed by Wild-Type and Variants of Triosephosphate Isomerase *J. Am. Chem. Soc.* **2019**, *141*, 16139−16150.[4] *The report of a linear correlation between $\Delta G^{\ddagger}$ and ΔG°, determined by electron valence bond calculations, for deprotonation of DHAP in water and when bound to wild-type or variants of TIM, to form the free or enzyme-stabilized enediolate reaction intermediate.*

1. INTRODUCTION

The Hammett equation was used to establish linear free energy relationships (LFERs) between the effect of aromatic ring substituents X on ΔG° for the reference ionization of substituted benzoic acids in water and on ΔG° or $\Delta G^{\ddagger}$ for reactions at second aromatic frameworks (Figure 1).[5] This

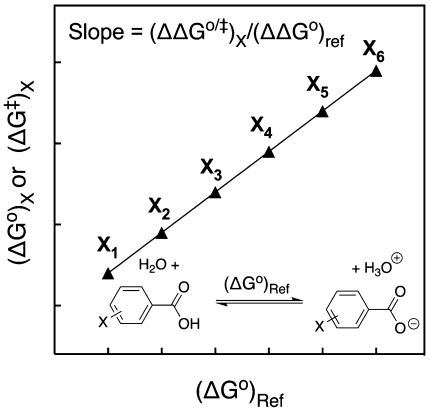

Figure 1. LFER between the effect of changing X on $(\Delta G^{\circ})_{ref}$ for the reference ionization of ring-substituted benzoic acids and on $(\Delta G^{\circ})_X$ or $(\Delta G^{\ddagger})_X$ for a second reaction at a similar rigid organic framework.

equation spurred the characterization of other LFERs, including those correlated by equations developed by Taft, Brønsted, and Grunwald and Winstein.[6] These LFERs are a cornerstone of physical organic chemistry.[7]

Figure 2A shows a pair of reactions for which a LFER is observed. The correlation between ΔG° for ionization of substituted phenylacetic and benzoic acids in water, with a slope of 0.5,[8] is consistent with a 2-fold falloff in electrostatic interactions between the ring substituent X and the reacting −COOH that arises from insertion of the methylene group. The slopes determined for Brønsted correlations of log k against the pK_a of varied reactants, such as Brønsted acid (slope of α) or base (slope of β) catalysts, or reacting alkyl alcohol nucleophiles (slope of β_{nuc}) or alkoxy leaving groups (slope of β_{lg}) generally lie between 0 and 1.0. These slopes provide a metric for the change in the effective charge "seen" by the varied substituent on proceeding to the reaction transition state, relative to the 1.0 unit change in the charge for the reference ionization reaction.[9]

Brønsted coefficients provide insight into changes in bonding interactions during steps that are not easily probed by kinetic experiments. For example, the value of $(\beta_{nuc})_{obs}$ = −0.1 determined for phosphoryl transfer from phosphorylated pyridine to 3-substituted quinuclidines in water requires a surprising decrease in the effective positive charge at the quinuclidine nitrogen at the transition state for the phosphoryl transfer reaction, so that the reacting amine nitrogen must carry a partial positive charge at the ground state in water.[10] These results were rationalized by Scheme 1, where β_{des} = −0.2 for removal of a hydrogen-bonded water from the tertiary amine nucleophile to form the desolvated encounter complex with the phosphorylated pyridine has a larger absolute value than $(\beta_{nuc})_{chem}$ = 0.1 for conversion of this encounter complex to the reaction transition state. There is a similar decrease in amine reactivity, with increasing amine basicity, for nucleophilic addition of amines to the 1-(methylthiophenyl)-2,2,2-trifluoroethyl carbocation.[11]

2. BEGINNINGS

J.P.R. first encountered the Brønsted equation in studies on addition of alkyl alcohols to ring-substituted 1-phenylethyl carbocations. The values of β_{nuc} for these reactions (Figure 2B, no general base catalysis), determined as the slopes of correlations of log k_X against alcohol pK_a, were found to increase from β_{nuc} = 0.1 to β_{nuc} = 0.5 as the carbocation is stabilized by a change in the aromatic ring substituent from Z = 4-CH_3 to 4-NMe_2 (Figure 2B).[12] This increase in the *effective* transition state positive charge at the oxygen nucleophile, with the decreasing thermodynamic driving force for carbocation addition, arises from a Hammond-type shift from a reactant to product-like transition state, where there is an increase in bonding between the oxygen nucleophile and carbon electrophile.[13]

These addition reactions of alcohols are catalyzed by alkane carboxylate anions, with third-order rate constants k_{YAc} (Figure 2B).[14,15] The slopes of Brønsted-type correlations of log k_{YAc} against the pK_a of the conjugate acid of the catalyst increase from β = 0.23 to β = 0.33 for addition of trifluoroethanol, as the aromatic ring substituent is changed from Z = 4-OCH_3 to 4-NMe_2.[15] This is consistent with an increase in transition state bonding between the alkane carboxylate base and the transferred alcohol proton (Figure 3A).[16]

Proton transfer from XCH_2CH_2OH to the carboxylate anion reduces the effective negative charge at the base catalyst and the effective positive charge at the oxygen nucleophile.[16] The latter change is reflected in the decrease in β_{nuc} = 0.5 for the uncatalyzed addition of alkyl alcohols to the 1-(4-dimethylaminophenyl)ethyl carbocation to β_{nuc} = 0.11 for the addition reaction catalyzed by acetate anion (Figure 3B).[15] These changes in first-derivative effects describe changes, with the changing reaction driving force, in the transition state structure: they define second-derivative effects. The results were modeled on a reaction coordinate profile, which assigns separate axes for bond formation between the alcohol oxygen and benzylic carbon, and for proton transfer from the alcohol

https://doi.org/10.1021/acs.accounts.1c00147
Acc. Chem. Res. 2021, 54, 2532−2542

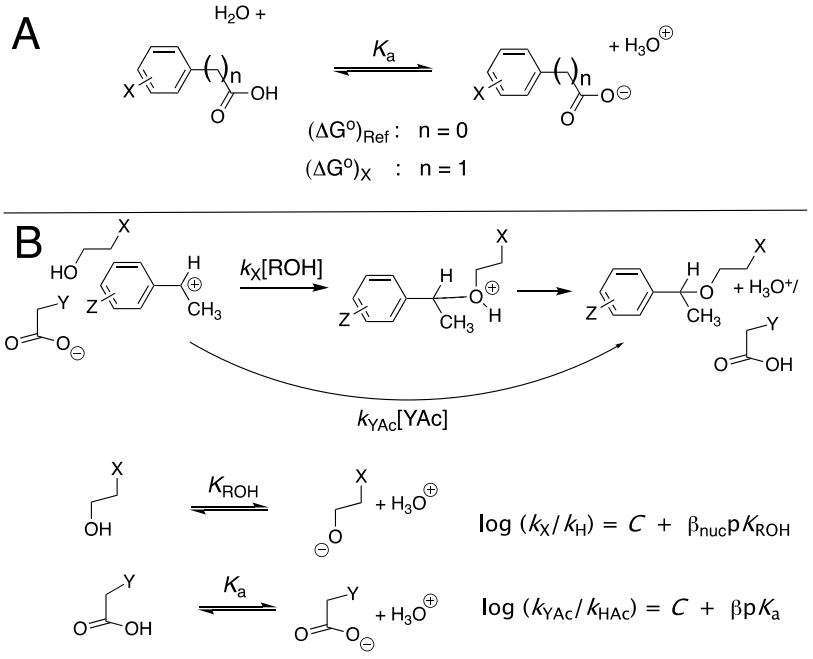

Figure 2. (A) The ionization of ring-substituted benzoic acids ($(\Delta G^{\circ})_{ref}$, n = 0) and phenylacetic acids ($(\Delta G^{\circ})_X$, n = 1). (B) Addition of substituted ethanols to ring-substituted 1-phenylethyl carbocations, with rate constants k_X (M^{-1} s^{-1}), to form protonated alkyl 1-phenylethyl ethers and general-base catalysis by alkane carboxylate anions of nucleophile addition, with rate constants k_{YAc} (M^{-2} s^{-1}), to form ring-substituted alkyl 1-phenylethyl ethers.

Scheme 1. Transfer of a Phosphoryl Group from Phosphorylated Pyridine to 3-Substituted Quinuclidines in Water

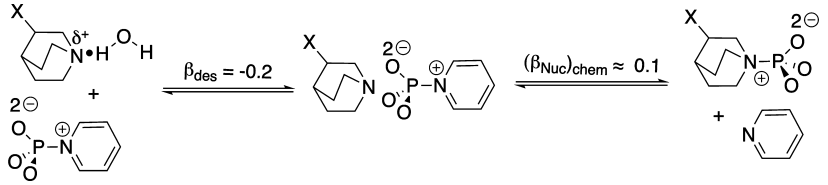

oxygen to the carboxylate anion,[17] using a protocol developed by William Jencks that expands upon a model from Bell, Marcus, Hammond, Polanyi, Thornton, and Leffler.[16]

3. EARLY STUDIES AT BUFFALO

Enzymes achieve rate accelerations through stabilization of their bound transition states by interactions with protein catalysts.[18−20] The structures of these transition states are of intellectual interest and may guide the development of tight-binding transition state analog enzyme inhibitors, with the potential to function as therapeutic agents.[21] The first step in β-galactosidase-catalyzed hydrolysis of alkyl β-D-galactopyranosides is transfer of the β-D-galactopyranosyl group from the substrate to the carboxylate side chain of E537 (Figure 4),[22,23] by a stepwise mechanism where the acidic E461 side chain provides Brønsted catalysis of glycoside bond cleavage to form the β-D-galactopyranosyl cation intermediate,[24] which is then trapped by the E537 side chain (Figure 4). The similarity between the transition states for the general base-catalyzed addition of alkyl alcohols to (i) ring-substituted 1-phenylethyl carbocations (Figures 3A and 3B) and (ii) the cation formed at β-galactosidase (Figure 3C) prompted studies to compare the structure−reactivity parameters determined for these enzymatic reactions and the nonenzymatic model.[25−27]

Figures 5A and 5B (●) show Brønsted plots of log k_{cat}/K_m and log k_{ROH} against alcohol pK_a, with slopes of β_{lg} = −0.75 and β_{nuc} = −0.19, respectively, for reversible β-galactosidase-catalyzed cleavage of alkyl β-galactopyranosides to form the alkyl alcohol and covalent reaction intermediate (Figure 4).[25,26] Figure 5C shows the plot of equilibrium constants log K_{eq} = log[(k_{cat}/K_m)/(k_{ROH})], with slope β_{eq} = −0.75 − (−0.19) = −0.56 for the β-D-galactopyranosyl group transfer from alkyl β-galactopyranosides to the enzyme.[25] The large negative β_{eq} of −0.56 shows that interactions between electron-withdrawing alkoxy substituents −X and the electron-deficient β-D-galactopyranosyl group or the reactant are destabilizing, compared to the interactions between these −X and the proton of the alcohol product. It is consistent with a sugar substituent that imparts an *effective* positive charge of +0.56 to the alkoxy oxygen relative to the normalized charge of 0.0 at the alcohol product.[9] The value $(\beta_{nuc})_{obs}$ = −0.19 for alcohol addition is consistent with an *effective* transition state negative charge of −0.19 at the alkoxy oxygen. This is equal to the sum of the contribution of the effective positive charge from the β-D-galactopyranosyl group plus the true formal negative charge at oxygen. The value of $(\beta_{nuc})_{obs}$ underestimates the buildup of the formal negative charge at this oxygen, because stabilizing charge interactions at oxygen are masked [canceled] by destabilizing dipole−dipole interactions between the electron-deficient sugar and electron-deficient substituents at XCH_2CH_2OH.

https://doi.org/10.1021/acs.accounts.1c00147
Acc. Chem. Res. 2021, 54, 2532−2542

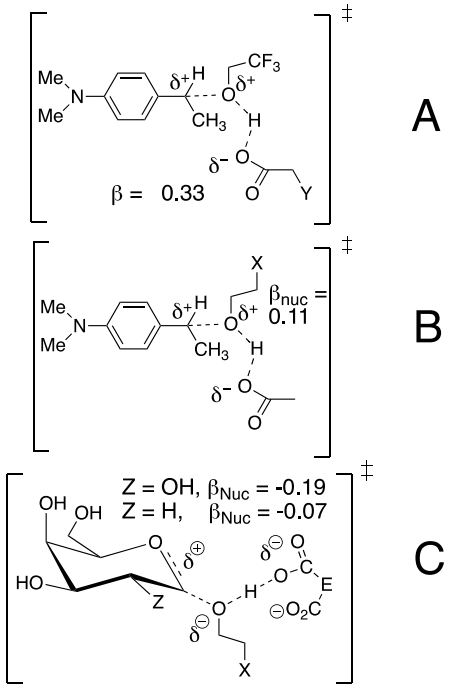

Figure 3. (A) Transition state for addition of trifluoroethanol to the 1-(4-dimethylaminophenyl)ethyl carbocation catalyzed by substituted alkane carboxylate anions (β = 0.33). (B) Transition state for the addition of substituted alkyl alcohols XCH_2CH_2OH to the 1-(4-dimethylaminophenyl)ethyl carbocation catalyzed by acetate anion. The value of β_{nuc} = 0.11 is consistent with the buildup of the positive charge at the nucleophilic oxygen. (C) Transition state for addition of XCH_2CH_2OH to the β-D-galactopyranosyl cation intermediate of reactions catalyzed by β-galactosidase. The values of β_{nuc} = −0.19 and β_{nuc} = −0.07 for Z = OH and Z = H, respectively, are consistent with a transition state where proton transfer from the alcohol to the enzyme is further advanced than bond formation between the alcohol and the sugar, leaving a net negative charge at the oxygen nucleophile.

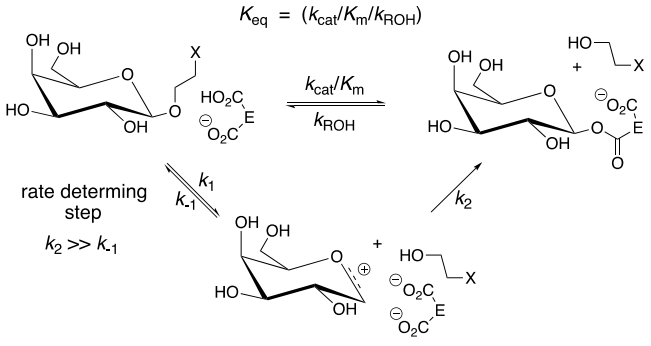

Figure 4. Stepwise β-galactosidase-catalyzed sugar transfer from alkyl β-D-galactopyranosides to the carboxylate side chain of E537, with Brønsted acid catalysis by the E461 side chain.

The value of β_{nuc} = −0.19 for alcohol addition to the glycosyl cation intermediate reflects the balance between bond development between the alkoxy oxygen and the glycosyl carbon and proton transfer from oxygen to the carboxylate catalyst. It is consistent with a strong coupling of changes in C−O and H−O bonding at the reaction transition state,[16] as was documented for catalysis of the reversible addition alkyl alcohols to formaldehyde and acetaldehyde.[28,29] A weaker coupling between these changes in bonding was determined for general base catalysis of alcohol addition to ring-substituted

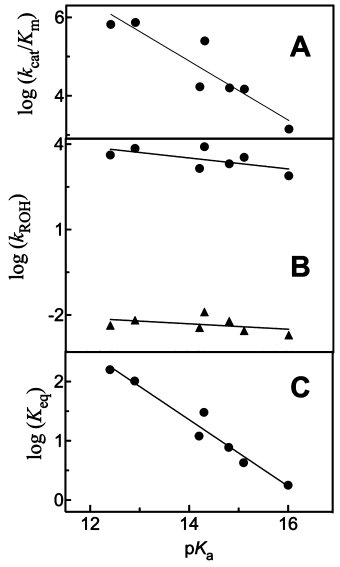

Figure 5. Brønsted correlations of kinetic parameters for β-galactosidase-catalyzed transfer of the β-D-galactopyranosyl group from alkyl β-D-galactopyranosides to the carboxylate side chain of E537, with rate-determining substrate ionization to form the glycosyl carbocation intermediate (Figure 4). (A) The correlation of rate constants (k_{cat}/K_m) for the reaction in the cleavage direction.[26] (B) Correlations of rate constants k_{ROH} for the reaction in the reverse, synthesis direction: (●) addition of alkyl alcohols to the β-D-galactopyranoside intermediate[25] and (▲) addition of alkyl alcohols to the 2-deoxy-β-D-galactopyranoside intermediate.[27] (c) The correlation of equilibrium constants K_{eq} for transfer of the β-D-galactopyranosyl group from the substrate to the enzyme.[25]

1-phenylethyl carbocations (β_{nuc} > 0, Figure 3B), where motion on the reaction coordinate at the transition state is dominated by formation of the C−O bond, with smaller movement of the proton toward the Brønsted base catalyst.[15]

The C-2 hydroxyl of the β-D-galactopyranosyl cation reaction intermediate stabilizes the transition state for β-galactosidase-catalyzed addition of trifluoroethanol by 7.6 kcal/mol.[30] This is accompanied by a decrease in β_{nuc} for alcohol addition from β_{nuc} = −0.07 (▲, Figure 5B) to β_{nuc} = −0.19 (●).[27] The decrease in β_{nuc}, with increasing stability of the glycosyl cation intermediate, corresponds to an anti-Hammond shift of the transition state toward reactants,[16] in contrast to the Hammond-type in the shift in the transition state observed for alcohol addition to ring-substituted-1-phenylethyl carbocations.[15,16] Anti-Hammond shifts in transition state structure have also been reported for general base catalysis of addition of alcohols to the carbonyl groups of formaldehyde and to acetaldehyde.[28,29] They were rationalized by a saddle point that shows a strongly coupled motion of the nucleophilic oxygen toward the carbon electrophile and of proton transfer from XCH_2CH_2OH to the base catalyst.[16] These differences in coupling observed for general base catalysis of alcohol addition to ring-substituted 1-phenylethyl carbocations, compared to formaldehyde and acetaldehyde, were proposed to arise because of changes in the curvature of the energy surface in the region of the saddle point on a two-dimensional reaction coordinate profile.[16,31] These results are consistent with a similar tight coupling of changes in bonding for addition of XCH_2CH_2OH to the protein-stabilized sugar carbocation intermediates of reactions catalyzed by β-galactosidase.[24,27]

https://doi.org/10.1021/acs.accounts.1c00147
Acc. Chem. Res. 2021, 54, 2532−2542

4. ENZYME CATALYSIS AT PROTEIN CAGES

The insight gained from studies on β-galactosidase has helped us to uncover LFERs of kinetic data for other enzymatic reactions. The transition states for decarboxylation catalyzed by orotidine 5′-monophosphate decarboxylase (OMPDC),[32,33] isomerization catalyzed by triosephosphate isomerase (TIM),[33−35] and hydride transfer catalyzed by glycerol 3-phosphate dehydrogenase (GPDH)[33,36] show a similar 12 kcal/mol stabilization by interactions with the phosphodianion of the whole substrate (Figure 6). This transition state

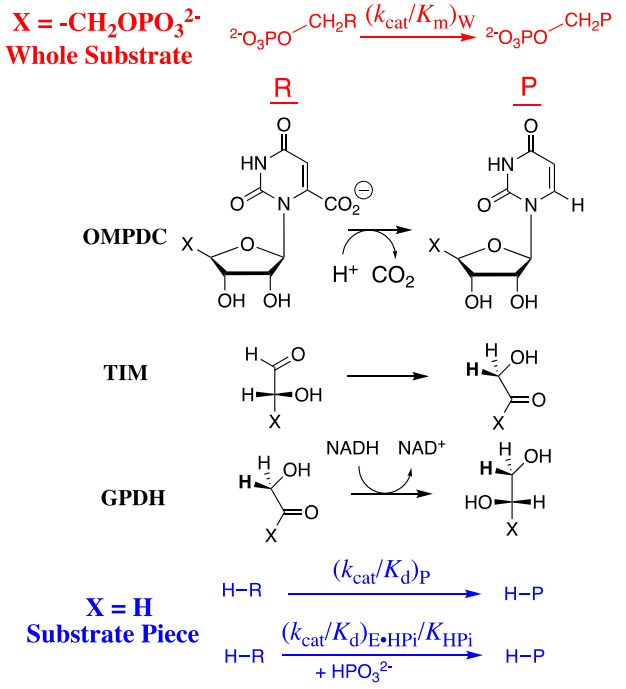

Figure 6. Reactions of whole substrates $[(k_{cat}/K_m)_W]$, the phosphodianion truncated substrate $[(k_{cat}/K_m)_P]$, and phosphite dianion activation of the truncated substrate $[(k_{cat}/K_dK_{HPi})]$ catalyzed by OMPDC, TIM, and GPDH.

stabilization is calculated from the ratio of second-order rate constants for the enzyme-catalyzed reactions of whole and phosphodianion truncated substrates: $[-RT \ln[(k_{cat}/K_m)_W/(k_{cat}/K_d)_P] = 12 \pm 1$ kcal/mol). In all three cases, the slow enzymatic reaction of the truncated substrate is strongly activated by the substrate piece phosphite dianion. This activation corresponds to a 6−8 kcal/mol stabilization of the transition states for reactions of truncated substrates by enzyme-bound phosphite dianion.

The 12 kcal/mol stabilization of these enzymatic transition states by interactions with the substrate phosphodianion shows the power of this small fragment to promote efficient enzymatic catalysis. The large fraction of these interactions specifically expressed at these transition states shows that TIM, OMPDC, and GPDH have evolved mechanisms that avoid the full expression of the strong ligand binding at the Michaelis complex, in order to avoid tight and irreversible binding of the substrate.[20,37,38] The observation of dianion activation of enzyme-catalyzed proton and hydride transfer and decarboxylation reactions is significant because such activation had not previously been considered for these three intensively studied enzymes. This suggests that [many] other exciting results await discovery by mechanistic enzymologists. At the very least, these results are the tip of the iceberg of enzymatic reactions for which there is a large specificity of nonreacting substrate fragments in the stabilization of the enzymatic transition state.[39]

The similarity in the kinetic results for activation of TIM, OMPDC, and GPDH by phosphite suggested a common mechanism for obtaining dianion specificity for transition state binding. The enzyme X-ray crystal structures provide the critical clue that reveals the mechanism of dianion activation. These structures show that TIM, OMPDC, and GPDH each utilizes phosphodianion binding energy to drive extensive conformational changes that are dominated by the closure of flexible phosphodianion gripper loops over the substrate.[3,40−44] Loop closure converts flexible open enzymes to closed Michaelis complexes, with the substrate trapped in a protein cage and sequestered from interaction with the solvent water.[45]

Scheme 2 shows a compelling model for dianion activation. The catalytic activity of the ground-state open form (E_O) of

Scheme 2. Enzyme Activation by a Ligand Driven Conformational Change that Converts an Inactive Open Enzyme (E_O) to the High Energy Catalytically Active Substrate Cage (E_C)

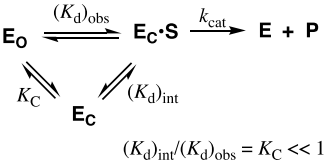

these three enzymes is low, compared to the active closed form E_C, because the side chains are poorly positioned for catalysis. The enzyme activity toward catalysis of reactions of phosphodianion truncated substrates is likewise low, because only a small fraction of total enzyme is present in the active closed conformation ($K_C \ll 1.0$), and there is insufficient substrate binding energy to drive the enzyme-activating conformational change. A high activity is observed for phosphorylated substrates and for the reactions of truncated substrates in the presence of phosphite dianion, because of utilization of dianion binding energy to convert these enzymes from inactive E_O to active E_C•S.[20,38,46] Scheme 2 is the induced fit mechanism that was proposed more than 60 years ago,[47] in another context, and whose significance has since been a subject of debate.[48] It provides a general mechanism for avoiding the full expression of binding interactions at the ground state Michaelis complex, through the utilization of substrate binding energy to drive formation of closed, high-energy, and catalytically active protein cages, where the number of stabilizing protein−ligand contacts has been optimized.[38,49] For example, OMPDC-catalyzed decarboxylation of OMP proceeds through a transition state that is stabilized by *ca.* 31 kcal/mol by interactions with the protein catalyst but with only a modest 8 kcal/mol stabilization of the Michaelis complex to OMP.[50] Much or all of this 23 kcal/mol difference represents the ligand binding energy utilized to drive the enzyme-activating conformational change from E_O to E_C.[41]

We have examined the mechanism for dianion activation in studies of variant enzymes prepared by site-directed mutagenesis. The positions of the active site side chains examined for yeast TIM are shown in Figure 7A for the complex to the phosphoglycolate (PGA) trianion.[51] Most of these side chains are buried beneath the phosphodianion gripper loop 6 (shaded

https://doi.org/10.1021/acs.accounts.1c00147
Acc. Chem. Res. 2021, 54, 2532−2542

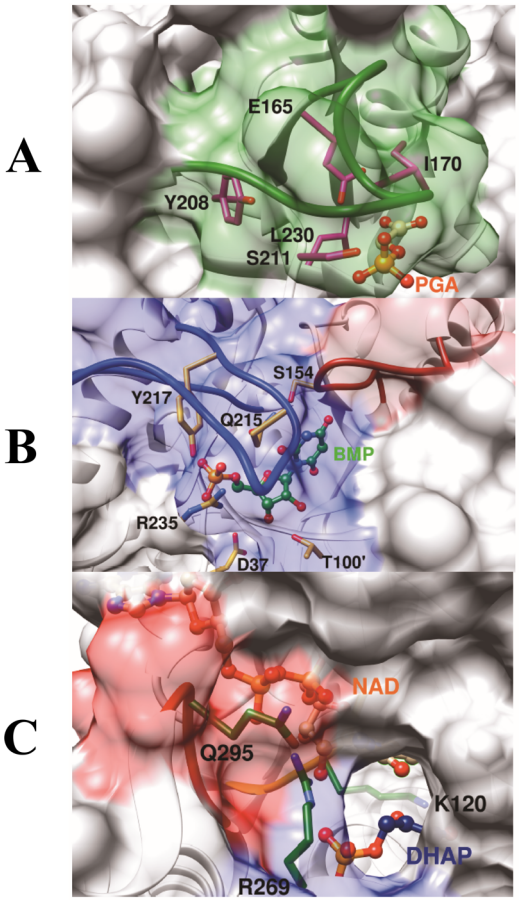

Figure 7. Representations from X-ray crystal structures of enzyme active sites, where the bound ligands are buried beneath the shaded protein surfaces: (A) The complex between TIM and PGA (PDB ID 2YPI). The phosphodianion gripper loop is shaded green. Figure 8 shows a correlation of kinetic parameters for wild-type TIMs and for the following enzyme variants: I170 V, I170A, Y208T, Y208A, Y208S, Y208F, Y208T/S211G, P166A, S211A, and S211G.[1,53] (B) The complex between OMPDC and 6-hydroxyuridine 5′-monophosphate (BMP, PDB ID 1DQX). The phosphodianion and pyrimidine gripper loops are shaded blue and pink, respectively. Figure 8 shows a correlation of kinetic parameters for wild-type OMPDC and the following variants: Q215A, Y217F, Q215A/R235A, R235A, S154A, and S154A/Q215A.[55] (C) The nonproductive complex between GPDH, NAD, and DHAP (PDB ID 6E90), with the flexible capping loop shaded red and additional surface residues shaded blue. Figure 8 shows a correlation of kinetic parameters for wild-type *hl*GPDH and for the following enzyme variants: Q295G, Q295S Q295A, Q295N, and K120A.[3,56]

green, Figure 7A) and play structural roles in optimizing the reactivity of the enzyme-bound substrate toward deprotonation.[1,52−54]

The kinetic parameters k_{cat}/K_m for catalysis of the reaction of the whole substrate and k_{cat}/K_dK_{HPi} for phosphite dianion activation of the catalyzed reactions of the substrate piece glycolaldehyde (Scheme 3) were determined for catalysis by TIM. We first focused on rationalizing the effects of individual mutations on these rate constants[57,58] but then noted an excellent linear free energy relationship, with a slope of 1.06 ± 0.04,[1] between the effect these substitutions have on log k_{cat}/K_m and log k_{cat}/K_dK_{HPi} (Figure 8 (●)). This correlation shows that the individual substitutions cause nearly the same change in the stability of the transition states for the two reactions. In

Scheme 3. Enzyme-Catalyzed Reactions of the Whole Substrate and Phosphite Dianion Activated Reactions of Truncated Substrates with Rate Constants k_{cat}/K_m (M^{-1} s^{-1}) and k_{cat}/K_dK_{HPi} (M^{-2} s^{-1}), Respectively

$$E_O + RCH_2\text{-}OPO_3^{2-} \overset{k_{cat}/K_m}{\rightleftharpoons} [E_C\cdot RCH_2OPO_3^{2-}]^{\ddagger} \longrightarrow E_O + PCH_2\text{-}OPO_3^{2-}$$

$$E_O + RH + HPO_3^{2-} \overset{k_{cat}/K_dK_{HPi}}{\rightleftharpoons} [E_C\cdot RH\cdot HPO_3^{2-}]^{\ddagger} \longrightarrow E_O + PH + HPO_3^{2-}$$

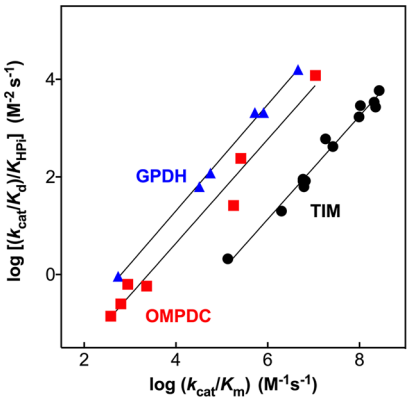

Figure 8. Linear free energy relationships between the effect of site-directed substitutions at TIM,[1] OMPDC,[55] and GPDH[3] on the kinetic parameters k_{cat}/K_m and k_{cat}/K_dK_{HPi} for enzyme-catalyzed reactions of whole and truncated substrates, respectively. The positions of the substituted side chains at the enzyme active sites are shown in Figure 7. The values of k_{cat}/K_m are for TIM-catalyzed isomerization of GAP, OMPDC-catalyzed decarboxylation of OMP, and GPDH-catalyzed reduction of dihydroxyacetone phosphate by NADH. The truncated substrates are glycolaldehyde (TIM and GPDH) and 1-(β-D-erythrofuranosyl)orotic acid (OMPDC).

other words, these transition states are nearly identical over the regions affected by these substitutions. There is a roughly constant difference of $\Delta\Delta G^{\ddagger} \approx 6.6$ kcal/mol in the activation barriers for TIM-catalyzed reactions of the whole substrate compared with the substrate pieces. This represents the entropic advantage to binding and reaction of the single whole substrate, compared with the two pieces.[1,53,59]

The correlation from Figure 8 was rationalized by Scheme 3. The interactions between TIM and the substrate phosphodianion, or the phosphite dianion piece, are utilized to drive the common enzyme conformational change from $\mathbf{E_O}$ to $\mathbf{E_C}$. This moves active-site side chains into positions that provide the same stabilization of the transition states for deprotonation of whole or truncated carbon acid substrates. The results of a high-level electron valence bond (EVB) computational study to model the reactivity of $\mathbf{E_C}$, using the X-ray structure of the Michaelis complex to DHAP,[44] gave similar activation barriers for deprotonation of enzyme-bound whole and truncated substrates to form the respective enediolate reaction intermediates. This is consistent with Scheme 2, where dianion binding interactions are utilized to stabilize a caged Michaelis complex, which shows the full catalytic activity toward deprotonation of both the truncated substrate glycolaldehyde and the whole substrate GAP.[60]

Figure 8 shows two additional LFERs between the values of log k_{cat}/K_m and log k_{cat}/K_dK_{HPi} (Scheme 3), with slopes of 1.065 ± 0.08 and 1.09 ± 0.03, respectively, for reactions catalyzed by wild-type and variant forms of OMPDC[55] and GPDH[3] (Figure 6), with the positions of the substituted side chains shown in Figures 7B and 7C, respectively. None of the

https://doi.org/10.1021/acs.accounts.1c00147
Acc. Chem. Res. 2021, 54, 2532−2542

side chains replaced act to directly stabilize the transition states for the respective wild-type enzyme-catalyzed reactions, except for the cationic side chain of K120 from GPDH, which provides electrostatic stabilization of the negative charge that develops at the transition state for enzyme-catalyzed hydride transfer from NADH to DHAP.[3,61] In the other cases, the side chains function to lock these enzymes into their closed conformations ($\mathbf{E}_C$), mainly though interactions with the substrate dianion. The near unit slopes for these correlations show that the amino-acid substitutions have nearly the same effect on the stability of the transition states for the enzyme-catalyzed reactions of whole substrates and the substrate pieces and are consistent with the conclusion that $\mathbf{E}_C$ shows nearly the same activity toward catalysis of reactions of whole substrates and the substrate pieces.[62−64] As noted above, this is predicted by the model shown in Scheme 2.

We have observed other linear free energy relationships for reactions catalyzed by TIM, OMPDC, and GPDH. For example, third-order rate constants k_{cat}/K_dK_X (M^{-2} s^{-1}) were determined for the activation of GPDH-catalyzed reactions of the truncated substrate glycolaldehyde by fluorophosphate, phosphite and sulfate dianion, and fourth-order rate constants $k_{cat}/K_dK_XK_{Gua}$ (M^{-3} s^{-1}) were determined for the activation of the R269A variant-catalyzed reaction by the combined effects of guanidine cation and each of the above three anions. The excellent LFER between values of log $k_{cat}/K_dK_XK_{Gua}$ and log k_{cat}/K_dK_X (not shown) for the reaction of these three dianions, with a slope of 1.0, shows that the R269A substitution does not significantly alter the interaction of these dianions with the enzyme-bound transition state complex, so that the structural integrity of the caged complex is maintained at the R269A variant.[63] Figure 9 shows a plot, with a slope of 0.95 and r^2 =

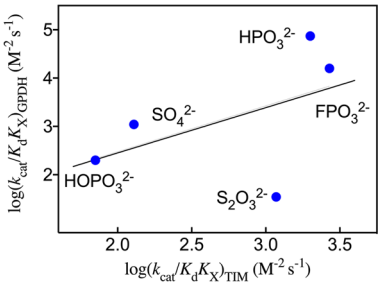

Figure 9. Correlation between third-order rate constants k_{cat}/K_dK_X (M^{-2} s^{-1}) for activation of GPDH and TIM by several tetrahedral dianions.[33]

0.26, for activation of TIM- and GPDH-catalyzed proton and hydride transfer reactions, respectively, by several different tetrahedral dianions. The poor quality of this correlation shows that there are significant differences in the stabilizing interactions of these different dianions at the active sites of TIM and GPDH.[33]

5. TRANSITION STATE ANALOGS

Enzyme catalysts show specificity in binding their transition states with a higher affinity than the substrate.[18] The tight binding observed for analogs of the transition states for enzymatic reactions provides evidence for this proposal.[65] The good linear correlation between values of log K_i for binding of phosphonoamidate peptide analogs (**1**) to thermolysin and log (k_{cat}/K_m) for thermolysin-catalyzed hydrolysis of the corresponding peptide substrates (**2**)[66] provides strong evidence that thermolysin stabilizes the covalent tetrahedral reaction intermediate formed by addition of water to the peptide substrate.

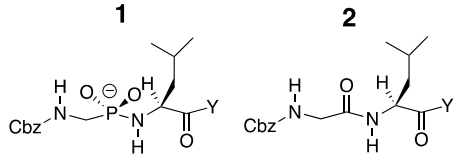

PGA binds to triosephosphate isomerase (K_i, Scheme 4) with a substantially higher affinity than substrates GAP and

Scheme 4. Inhibition of TIM by PGA

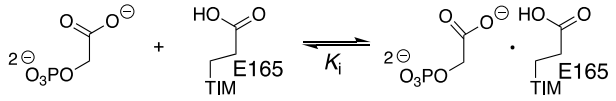

DHAP[65] and is a putative analog of the enediolate reaction intermediate (Scheme 4).[67] Figure 10 shows the correlation,

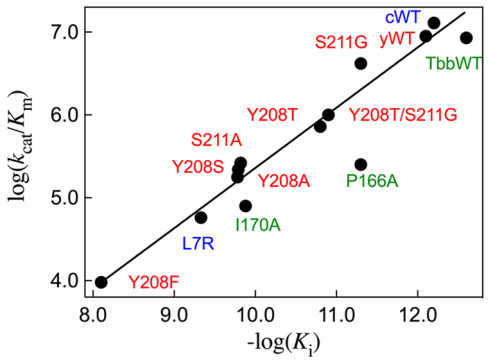

Figure 10. Linear logarithmic correlation between values of K_i for the breakdown of PGA-TIM complexes (Scheme 4) and k_{cat}/K_m for isomerization of GAP catalyzed by wild-type TIM from yeast (yTIM) and chicken muscle (cTIM) *Trypanosoma brucei* (TbbTIM) and by variant forms of these enzymes.[2]

with a slope of 0.73 (r^2 = 0.96), between values of log K_i and log k_{cat}/K_m for the isomerization of GAP catalyzed by wild-type and variants of TIM.[2] This correlation shows that the amino acid side chains substituted for at TIM (Figure 7) act to stabilize the complex between the enzyme and PGA trianion and that *ca.* 70% of this stabilization is observed at the transition state for substrate deprotonation.[2]

The binding of the PGA trianion to TIM results in an a > 6 unit increase in the pK_a of the E165 side chain, from pK_a = 4 at free TIM to pK_a > 10 at the complex to PGA (Figure 11).[2,68] This is due to the combined effects of stabilization of the inhibitor complex by a hydrogen bond between the PGA trianion and the protonated E165 side chain and destabilizing electrostatic interactions between the inhibitor trianion and the ionized side chain anion. A similar increase in the pK_a for this side chain should occur upon proton transfer from the carbon acid substrate to the E165 carboxylate, to form the enediolate anion reaction intermediate (Scheme 5 and Figure 11).[2,68] The high basicity of the E165 side chain at the complex to the enediolate reaction intermediate analog PGA [$(pK_a)_{COOH}$, Figure 11] reflects the tight packing of PGA into the solvent-

https://doi.org/10.1021/acs.accounts.1c00147
Acc. Chem. Res. 2021, 54, 2532−2542

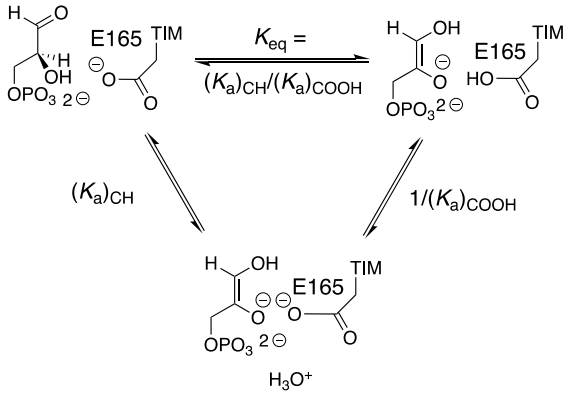

Figure 11. Deprotonation of TIM-bound GAP by the E165 active site side chain with equilibrium constant K_{eq}, where $K_{eq} = [(K_a)_{CH}/(K_a)_{COOH}]$ for proton transfer between the enzyme-reactant or enzyme-intermediate complex and water.

Scheme 5. Deprotonation of DHAP by Propionate in Water (Top Reaction) and by the Carboxylate Side Chain of E165 at the Active Site of Triosephosphate Isomerase

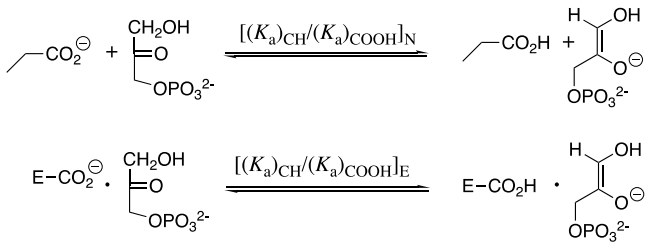

sequestered enzyme active site.[45,69,70] This promotes formation of the enediolate intermediate, provided that the enhanced side-chain basicity is expressed at the transition state for substrate deprotonation.[71] This model is supported by the observation that several side-chain substitutions at TIM, which result in decreases in log K_i for inhibition by PGA (Figure 10), also result in decreases in $(pK_a)_{COOH}$ (Figure 11) for the E165 side chain at the complex to PGA.[2,68]

6. IMPERATIVES FOR CATALYSIS OF DEPROTONATION OF CARBON

The activation barrier $\Delta G^{\ddagger}$ for nonenzymatic deprotonation of the relatively weak carbon acid DHAP ($pK_{CH} \approx 18$) by the weak base propionate anion ($pK_{COOH} \approx 5$, Scheme 5) is the sum of the thermodynamic reaction barrier ΔG° for proton transfer plus the contribution from the intrinsic kinetic reaction barrier Λ.[72] It is not clear that Λ may be reduced for reactions at enzyme active sites compared to water, and attention has been focused on quantifying the reduction in ΔG°. EVB calculations to determine $\Delta G^{\ddagger}$ and ΔG° for deprotonation of DHAP bound to wild-type and variant forms of TIM to form the enediolate reaction intermediate give the linear free energy correlation shown in Figure 12, with a slope of 0.74 (r^2 = 0.99).[4] The agreement between the computed activation barriers $\Delta G^{\ddagger}$ and the experimental barriers estimated from k_{cat} for TIM-catalyzed isomerization of GAP is within ±1 kcal/mol.

The substituted amino acid side chains at TIM (Figure 12) play a role in either maintaining the strong basicity of E165 (I170A, P166A, and L230A)[2,68] or in the direct stabilization of the enediolate intermediate (K12 and E97).[73] The Brønsted-

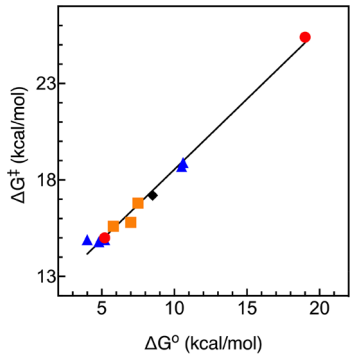

Figure 12. Linear free energy relationship between the calculated activation barrier $\Delta G^{\dagger}$ and the reaction free energy ΔG° for proton transfer from DHAP to propionate anion, wild-type TIM, and variants of TIM.[4] Key: ●, reactions catalyzed by wild-type TIM and propionate anion; ■, I170A and L230A variants; ▲, K12G and E97 variants; ♦, P166A variant.[4]

type correlation shows that these active site side chains function to reduce ΔG° for deprotonation of the weakly acidic α-carbonyl carbon acid substrate to form the enediolate phosphate trianion intermediate (Scheme 5) and that *ca.* 70% of this stabilization is expressed at the transition state for formation of this intermediate and as a decrease in $\Delta G^{\ddagger}$. These results provide evidence that proton transfer from the substrate to TIM is promoted by placement of active site side chains at positions which impart an optimal basicity to the E165 side chain and optimal stabilization of the negative charge at the reaction intermediate.[4]

7. CONCLUDING REMARKS

The transformation of tables of numerical rate data into graphical LFERs often brings clarity to kinetic analyses. At the very least, these LFERs provide a framework for discussion that may reveal differences in the interpretation and conclusions of studies on reaction mechanisms. These conversations sometimes motivate additional experiments that provide a spark for progress.

The early work on β-galactosidase-catalyzed glycosyl transfer reactions represented an attempt to extend classical applications of LFERs to studies on enzyme catalysis. Our interest in LFERs then decreased, as the focus of our research shifted to more traditional studies on enzymatic catalysis. However, the opportunities discussed in this Account have resulted in the seamless incorporation of LFERs into analyses of kinetic and computational data pertinent to the effect of active-site directed substitutions on enzyme kinetic parameters. We now understand that LFERs may be observed for kinetic data that correlate the effect of protein substitutions on the rate and/or equilibrium constants for enzymatic reactions, with the caveat that the active-site substitutions are not accompanied by nonspecific changes in protein structure; and note that similar relationships have featured strongly in the work of Fersht[74] and Auerbach.[75] The few examples presented here illustrate the potential of LFERs as tools for the analysis and interpretation of kinetic data for enzymatic reactions. We encourage others to search for additional relationships in their studies on enzymatic reaction mechanisms.

https://doi.org/10.1021/acs.accounts.1c00147
Acc. Chem. Res. 2021, 54, 2532−2542

AUTHOR INFORMATION

Corresponding Author

John P. Richard − *Department of Chemistry, University at Buffalo, SUNY, Buffalo, New York 14260-3000, United States*; orcid.org/0000-0002-0440-2387; Email: jrichard@buffalo.edu

Authors

Judith R. Cristobal − *Department of Chemistry, University at Buffalo, SUNY, Buffalo, New York 14260-3000, United States*

Tina L. Amyes − *Department of Chemistry, University at Buffalo, SUNY, Buffalo, New York 14260-3000, United States*

Complete contact information is available at: https://pubs.acs.org/10.1021/acs.accounts.1c00147

Notes

The authors declare no competing financial interest.

Biographies

John P. Richard received a B.S. degree (1974) in biochemistry at Ohio State and a Ph.D. degree (1979) in chemistry at the same University under the direction of Perry A. Frey. He was introduced to linear free energy relationships by his postdoctoral advisor William P. Jencks. He is currently a SUNY Distinguished Professor of Chemistry at the University at Buffalo, SUNY.

Judith R. Cristobal received her B.S. degree in chemistry (2009) from the University of the Philippines Los Baños and taught chemistry at this University from 2009−2016. She is currently a Ph.D. candidate at the University at Buffalo, SUNY.

Tina L. Amyes received B.A. and M.A. degrees in natural sciences and her Ph.D. degree in chemistry (1986) from the University of Cambridge (England). She currently works as a Scientific Program Manager at the Roswell Park Cancer Institute.

ACKNOWLEDGMENTS

The work described in this Account was supported by the following grants from the US National Institutes of Health: GM134881, GM116921, GM47307, and GM039754.

REFERENCES

(1) Zhai, X.; Amyes, T. L.; Richard, J. P. Role of Loop-Clamping Side Chains in Catalysis by Triosephosphate Isomerase. *J. Am. Chem. Soc.* **2015**, *137*, 15185−15197.

(2) Zhai, X.; Reinhardt, C. J.; Malabanan, M. M.; Amyes, T. L.; Richard, J. P. Enzyme Architecture: Amino Acid Side-Chains That Function To Optimize the Basicity of the Active Site Glutamate of Triosephosphate Isomerase. *J. Am. Chem. Soc.* **2018**, *140*, 8277−8286.

(3) Mydy, L. S.; Cristobal, J.; Katigbak, R.; Bauer, P.; Reyes, A. C.; Kamerlin, S. C. L.; Richard, J. P.; Gulick, A. M. Human Glycerol 3-Phosphate Dehydrogenase: X-Ray Crystal Structures that Guide the Interpretation of Mutagenesis Studies. *Biochemistry* **2019**, *58*, 1061−1073.

(4) Kulkarni, Y. S.; Amyes, T. L.; Richard, J. P.; Kamerlin, S. C. L. Uncovering the Role of Key Active-Site Side Chains in Catalysis: An Extended Brønsted Relationship for Substrate Deprotonation Catalyzed by Wild-Type and Variants of Triosephosphate Isomerase. *J. Am. Chem. Soc.* **2019**, *141*, 16139−16150.

(5) Hammett, L. P. The Effect of Structure upon the Reactions of Organic Compounds. Benzene Derivatives. *J. Am. Chem. Soc.* **1937**, *59*, 96−103.

(6) Leffler, E.; Grunwald, J. E.: *Rates and Equilibria of Organic Reactions*; John Wiley & Sons: New York, 1963.

(7) Williams, A.: *Free Energy Relationships in Organic and Bioorganic Chemistry*; Royal Society of Chemistry: Cambridge, 2003; DOI: 10.1039/9781847550927

(8) Dippy, J. F. J.; Watson, H. B.; Williams, F. R. Chemical constitution and the dissociation constants of mono-carboxylic acids. Part IV. A discussion of the electrolytic dissociation of substituted benzoic and phenylacetic acids in relation to other side-chain processes. *J. Chem. Soc.* **1935**, 346−350.

(9) Williams, A. Effective charge and transition-state structure in solution. *Adv. Phys. Org. Chem.* **1992**, *27*, 1−55.

(10) Jencks, W. P.; Haber, M. T.; Herschlag, D.; Nazaretian, K. L. Decreasing reactivity with increasing nucleophile basicity. The effect of solvation on β_{nuc} for phosphoryl transfer to amines. *J. Am. Chem. Soc.* **1986**, *108*, 479−483.

(11) Richard, J. P. Desolvation-limited reactions of amines with the 1-(4-methylthiophenyl)-2,2,2-trifluoroethyl carbocation. *J. Chem. Soc., Chem. Commun.* **1987**, 1768−1769.

(12) Richard, J. P.; Jencks, W. P. Reactions of substituted 1-phenylethyl carbocations with alcohols and other nucleophilic reagents. *J. Am. Chem. Soc.* **1984**, *106*, 1373−1383.

(13) Hammond, G. S. A Correlation of Reaction Rates. *J. Am. Chem. Soc.* **1955**, *77*, 334−338.

(14) Richard, J. P.; Jencks, W. P. General base catalysis of the addition of hydroxylic reagents to unstable carbocations and its disappearance. *J. Am. Chem. Soc.* **1984**, *106*, 1396−1401.

(15) Ta-Shma, R.; Jencks, W. P. How does a reaction change its mechanism? General base catalysis of the addition of alcohols to 1-phenylethyl carbocations. *J. Am. Chem. Soc.* **1986**, *108*, 8040−8050.

(16) Jencks, W. P. A primer for the Bema Hapothle. An empirical approach to the characterization of changing transition-state structures. *Chem. Rev.* **1985**, *85*, 511−527.

(17) More O'Ferrall, R. A. Relationships between E2 and $E1_{cb}$ Mechanisms of β-elimination. *J. Chem. Soc. B* **1970**, *0*, 274−277.

(18) Pauling, L. The nature of forces between large molecules of biological interest. *Nature* **1948**, *161*, 707−709.

(19) Wolfenden, R.; Snider, M. J. The Depth of Chemical Time and the Power of Enzymes as Catalysts. *Acc. Chem. Res.* **2001**, *34*, 938−945.

(20) Amyes, T. L.; Richard, J. P. Specificity in transition state binding: The Pauling model revisited. *Biochemistry* **2013**, *52*, 2021−2035.

(21) Schramm, V. L. Enzymatic Transition States and Drug Design. *Chem. Rev.* **2018**, *118*, 11194−11258.

(22) Gebler, J. C.; Aebersold, R.; Withers, S. Glu-537, Not Glu-461, Is the Nucleophile in the Active Site of *(lac Z)* β-Galactosidase from *Escherichia coli*. *J. Biol. Chem.* **1992**, *267*, 11126−11130.

(23) Yuan, J.; Martinez-Bilbao, M.; Huber, R. E. Substitutions of β-galactosidase from *Escherichia coli* cause large decreases in catalytic activity. *Biochem. J.* **1994**, *299*, 527−531.

(24) Richard, J. P.; Huber, R. E.; Heo, C.; Amyes, T. L.; Lin, S. Structure-reactivity relationships for β-galactosidase (Escherichia coli, lac Z). 4. Mechanism for reaction of nucleophiles with the galactosyl-enzyme intermediates of E461G and E461Q β-galactosidases. *Biochemistry* **1996**, *35*, 12387−12401.

(25) Richard, J. P.; Westerfeld, J. G.; Lin, S.; Beard, J. Structure-reactivity relationships for β-galactosidase (Escherichia coli, lac Z). 2. Reactions of the galactosyl-enzyme intermediate with alcohols and azide ion. *Biochemistry* **1995**, *34*, 11713−11724.

(26) Richard, J. P.; Westerfeld, J. G.; Lin, S. Structure-reactivity relationships for β-galactosidase (Escherichia coli, lac Z). 1. Brønsted parameters for cleavage of alkyl β-D-galactopyranosides. *Biochemistry* **1995**, *34*, 11703−11712.

(27) Richard, J. P.; Heo, C. K.; Toteva, M. M. Structure-reactivity relationships for β-galactosidase (Escherichia coli, lac Z): a second derivative effect on β_{nuc} for addition of alkyl alcohols to an oxocarbenium ion reaction intermediate. *J. Phys. Org. Chem.* **2008**, *21*, 531−537.

(28) Funderburk, L. H.; Aldwin, L.; Jencks, W. P. Mechanisms of general acid and base catalysis of the reactions of water and alcohols with formaldehyde. *J. Am. Chem. Soc.* **1978**, *100*, 5444−5459.
(29) Sorensen, P. E.; Jencks, W. P. Acid- and base-catalyzed decomposition of acetaldehyde hydrate and hemiacetals in aqueous solution. *J. Am. Chem. Soc.* **1987**, *109*, 4675−4690.
(30) Richard, J. P.; McCall, D. A.; Heo, C. K.; Toteva, M. M. Ground-state, transition-state, and metal-cation effects of the 2-hydroxyl group on β-D-galactopyranosyl transfer catalyzed by β-galactosidase (Escherichia coli, lac Z). *Biochemistry* **2005**, *44*, 11872−11881.
(31) Jencks, D. A.; Jencks, W. P. The characterization of transition states by structure-reactivity coefficients. *J. Am. Chem. Soc.* **1977**, *99*, 7948−7960.
(32) Amyes, T. L.; Richard, J. P.; Tait, J. J. Activation of orotidine 5′-monophosphate decarboxylase by phosphite dianion: The whole substrate is the sum of two parts. *J. Am. Chem. Soc.* **2005**, *127*, 15708−15709.
(33) Reyes, A. C.; Zhai, X.; Morgan, K. T.; Reinhardt, C. J.; Amyes, T. L.; Richard, J. P. The Activating Oxydianion Binding Domain for Enzyme-Catalyzed Proton Transfer, Hydride Transfer and Decarboxylation: Specificity and Enzyme Architecture. *J. Am. Chem. Soc.* **2015**, *137*, 1372−1382.
(34) Amyes, T. L.; Richard, J. P. Enzymatic catalysis of proton transfer at carbon: activation of triosephosphate isomerase by phosphite dianion. *Biochemistry* **2007**, *46*, 5841−5854.
(35) Amyes, T. L.; O'Donoghue, A. C.; Richard, J. P. Contribution of phosphate intrinsic binding energy to the enzymatic rate acceleration for triosephosphate isomerase. *J. Am. Chem. Soc.* **2001**, *123*, 11325−11326.
(36) Tsang, W.-Y.; Amyes, T. L.; Richard, J. P. A Substrate in Pieces: Allosteric Activation of Glycerol 3-Phosphate Dehydrogenase (NAD^+) by Phosphite Dianion. *Biochemistry* **2008**, *47*, 4575−4582.
(37) Jencks, W. P. Binding energy, specificity, and enzymic catalysis: the Circe effect. *Adv. Enzymol. Relat. Areas Mol. Biol.* **2006**, *43*, 219−410.
(38) Richard, J. P. Protein Flexibility and Stiffness Enable Efficient Enzymatic Catalysis. *J. Am. Chem. Soc.* **2019**, *141*, 3320−3331.
(39) Fernandez, P. L.; Nagorski, R. W.; Cristobal, J. R.; Amyes, T. L.; Richard, J. P. Phosphodianion Activation of Enzymes for Catalysis of Central Metabolic Reactions. *J. Am. Chem. Soc.* **2021**, *143*, 2694−2698.
(40) Ou, X.; Ji, C.; Han, X.; Zhao, X.; Li, X.; Mao, Y.; Wong, L.-L.; Bartlam, M.; Rao, Z. Crystal structures of human glycerol 3-phosphate dehydrogenase 1 (GPD1). *J. Mol. Biol.* **2006**, *357*, 858−869.
(41) Miller, B. G.; Hassell, A. M.; Wolfenden, R.; Milburn, M. V.; Short, S. A. Anatomy of a proficient enzyme: the structure of orotidine 5′-monophosphate decarboxylase in the presence and absence of a potential transition state analog. *Proc. Natl. Acad. Sci. U. S. A.* **2000**, *97*, 2011−2016.
(42) Lolis, E.; Petsko, G. A. Crystallographic analysis of the complex between triosephosphate isomerase and 2-phosphoglycolate at 2.5-Å resolution: implications for catalysis. *Biochemistry* **1990**, *29*, 6619−6625.
(43) Chan, K. K.; Wood, B. M.; Fedorov, A. A.; Fedorov, E. V.; Imker, H. J.; Amyes, T. L.; Richard, J. P.; Almo, S. C.; Gerlt, J. A. Mechanism of the Orotidine 5′-Monophosphate Decarboxylase-Catalyzed Reaction: Evidence for Substrate Destabilization. *Biochemistry* **2009**, *48*, 5518−5531.
(44) Jogl, G.; Rozovsky, S.; McDermott, A. E.; Tong, L. Optimal alignment for enzymatic proton transfer: structure of the Michaelis complex of triosephosphate isomerase at 1.2-Å resolution. *Proc. Natl. Acad. Sci. U. S. A.* **2003**, *100*, 50−55.
(45) Richard, J. P.; Amyes, T. L.; Goryanova, B.; Zhai, X. Enzyme architecture: on the importance of being in a protein cage. *Curr. Opin. Chem. Biol.* **2014**, *21*, 1−10.
(46) Go, M. K.; Amyes, T. L.; Richard, J. P. Hydron Transfer Catalyzed by Triosephosphate Isomerase. Products of the Direct and Phosphite-Activated Isomerization of [1-^{13}C]-Glycolaldehyde in D_2O. *Biochemistry* **2009**, *48*, 5769−5778.
(47) Koshland, D. E., Jr. Application of a Theory of Enzyme Specificity to Protein Synthesis. *Proc. Natl. Acad. Sci. U. S. A.* **1958**, *44*, 98−104.
(48) Herschlag, D. The role of induced fit and conformational changes of enzymes in specificity and catalysis. *Bioorg. Chem.* **1988**, *16*, 62−96.
(49) Amyes, T. L.; Malabanan, M. M.; Zhai, X.; Reyes, A. C.; Richard, J. P. Enzyme activation through the utilization of intrinsic dianion binding energy. *Prot. Eng., Des. Sel.* **2017**, *30*, 157−165.
(50) Richard, J. P.; Amyes, T. L.; Reyes, A. C. Orotidine 5′-Monophosphate Decarboxylase: Probing the Limits of the Possible for Enzyme Catalysis. *Acc. Chem. Res.* **2018**, *51*, 960−969.
(51) Lolis, E.; Petsko, G. A. Crystallographic analysis of the complex between triosephosphate isomerase and 2-phosphoglycolate at 2.5-Å resolution: implications for catalysis. *Biochemistry* **1990**, *29*, 6619−6625.
(52) Zhai, X.; Go, M. K.; Donoghue, A. C.; Amyes, T. L.; Pegan, S. D.; Wang, Y.; Loria, J. P.; Mesecar, A. D.; Richard, J. P. Enzyme Architecture: The Effect of Replacement and Deletion Mutations of Loop 6 on Catalysis by Triosephosphate Isomerase. *Biochemistry* **2014**, *53*, 3486−3501.
(53) Zhai, X.; Amyes, T. L.; Richard, J. P. Enzyme Architecture: Remarkably Similar Transition States for Triosephosphate Isomerase-Catalyzed Reactions of the Whole Substrate and the Substrate in Pieces. *J. Am. Chem. Soc.* **2014**, *136*, 4145−4148.
(54) Zhai, X.; Amyes, T. L.; Wierenga, R. K.; Loria, J. P.; Richard, J. P. Structural Mutations That Probe the Interactions between the Catalytic and Dianion Activation Sites of Triosephosphate Isomerase. *Biochemistry* **2013**, *52*, 5928−5940.
(55) Goldman, L. M.; Amyes, T. L.; Goryanova, B.; Gerlt, J. A.; Richard, J. P. Enzyme Architecture: Deconstruction of the Enzyme-Activating Phosphodianion Interactions of Orotidine 5′-Monophosphate Decarboxylase. *J. Am. Chem. Soc.* **2014**, *136*, 10156−10165.
(56) He, R.; Reyes, A. C.; Amyes, T. L.; Richard, J. P. Enzyme Architecture: The Role of a Flexible Loop in Activation of Glycerol-3-phosphate Dehydrogenase for Catalysis of Hydride Transfer. *Biochemistry* **2018**, *57*, 3227−3236.
(57) Malabanan, M. M.; Koudelka, A. P.; Amyes, T. L.; Richard, J. P. Mechanism for Activation of Triosephosphate Isomerase by Phosphite Dianion: The Role of a Hydrophobic Clamp. *J. Am. Chem. Soc.* **2012**, *134*, 10286−10298.
(58) Malabanan, M. M.; Amyes, T. L.; Richard, J. P. Mechanism for Activation of Triosephosphate Isomerase by Phosphite Dianion: The Role of a Ligand-Driven Conformational Change. *J. Am. Chem. Soc.* **2011**, *133*, 16428−16431.
(59) Jencks, W. P. On the attribution and additivity of binding energies. *Proc. Natl. Acad. Sci. U. S. A.* **1981**, *78*, 4046−4050.
(60) Kulkarni, Y. S.; Liao, Q.; Byléhn, F.; Amyes, T. L.; Richard, J. P.; Kamerlin, S. C. L. Role of Ligand-Driven Conformational Changes in Enzyme Catalysis: Modeling the Reactivity of the Catalytic Cage of Triosephosphate Isomerase. *J. Am. Chem. Soc.* **2018**, *140*, 3854−3857.
(61) He, R.; Cristobal, J. R.; Gong, N. J.; Richard, J. P. Hydride Transfer Catalyzed by Glycerol Phosphate Dehydrogenase: Recruitment of an Acidic Amino Acid Side Chain to Rescue a Damaged Enzyme. *Biochemistry* **2020**, *59*, 4856−4863.
(62) Cristobal, J. R.; Reyes, A. C.; Richard, J. P. The Organization of Active Site Side Chains of Glycerol-3-phosphate Dehydrogenase Promotes Efficient Enzyme Catalysis and Rescue of Variant Enzymes. *Biochemistry* **2020**, *59*, 1582−1591.
(63) Reyes, A. C.; Amyes, T. L.; Richard, J. P. Enzyme Architecture: Self-Assembly of Enzyme and Substrate Pieces of Glycerol-3-Phosphate Dehydrogenase into a Robust Catalyst of Hydride Transfer. *J. Am. Chem. Soc.* **2016**, *138*, 15251−15259.
(64) Reyes, A. C.; Koudelka, A. P.; Amyes, T. L.; Richard, J. P. Enzyme Architecture: Optimization of Transition State Stabilization

https://doi.org/10.1021/acs.accounts.1c00147
Acc. Chem. Res. 2021, 54, 2532−2542

from a Cation−Phosphodianion Pair. *J. Am. Chem. Soc.* **2015**, *137*, 5312−5315.
(65) Wolfenden, R. Transition State Analogues for Enzyme Catalysis. *Nature* **1969**, *223*, 704−705.
(66) Bartlett, P. A.; Marlowe, C. K. Phosphonamidates as transition-state analog inhibitors of thermolysin. *Biochemistry* **1983**, *22*, 4618−4624.
(67) Campbell, I. D.; Jones, R. B.; Kiener, P. A.; Waley, S. G. Enzyme-substrate and enzyme-inhibitor complexes of triose phosphate isomerase studied by 31P nuclear magnetic resonance. *Biochem. J.* **1979**, *179*, 607−621.
(68) Malabanan, M. M.; Nitsch-Velasquez, L.; Amyes, T. L.; Richard, J. P. Magnitude and origin of the enhanced basicity of the catalytic glutamate of triosephosphate isomerase. *J. Am. Chem. Soc.* **2013**, *135*, 5978−5981.
(69) O'Donoghue, A. C.; Amyes, T. L.; Richard, J. P. Hydron Transfer Catalyzed by Triosephosphate Isomerase. Products of Isomerization of Dihydroxyacetone Phosphate in D_2O. *Biochemistry* **2005**, *44*, 2622−2631.
(70) O'Donoghue, A. C.; Amyes, T. L.; Richard, J. P. Hydron Transfer Catalyzed by Triosephosphate Isomerase. Products of Isomerization of (R)-Glyceraldehyde 3-Phosphate in D_2O. *Biochemistry* **2005**, *44*, 2610−2621.
(71) Richard, J. P. The Enhancement of Enzymic Rate Accelerations by Brønsted Acid-Base Catalysis. *Biochemistry* **1998**, *37*, 4305−4309.
(72) Gerlt, J. A.; Gassman, P. G. An explanation for rapid enzyme-catalyzed proton abstraction from carbon acids: importance of late transition states in concerted mechanisms. *J. Am. Chem. Soc.* **1993**, *115*, 11552−11568.
(73) Go, M. K.; Koudelka, A.; Amyes, T. L.; Richard, J. P. Role of Lys-12 in Catalysis by Triosephosphate Isomerase: A Two-Part Substrate Approach. *Biochemistry* **2010**, *49*, 5377−5389.
(74) Fersht, A. R.; Wells, T. N. C. Linear free energy relationships in enzyme binding interactions studied by protein engineering. *Protein Eng., Des. Sel.* **1991**, *4*, 229−231.
(75) Cymes, G. D.; Grosman, C.; Auerbach, A. Structure of the Transition State of Gating in the Acetylcholine Receptor Channel Pore: A Φ-Value Analysis. *Biochemistry* **2002**, *41*, 5548−5555.

https://doi.org/10.1021/acs.accounts.1c00147
Acc. Chem. Res. 2021, 54, 2532−2542